碩士學位論文

Determination of Void Fraction in Concentric Annular and Stratified Two Phase Flows Using Impedance Technique

임피던스 기법을 이용한 환상 및 성층류 유동에서의 기포율 결정

濟州大學校 大學院

에너지 工學科

高 敏 碩

2010年 12月

Determination of Void Fraction in Concentric Annular and Stratified Two Phase Flows Using Impedance Technique

임피던스 기법을 이용한 환상 및 성층류 유동에서의 기포율 결정

指導教授 金 信

高 敏 碩

이 論文을 工學 碩士學位 論文으로 提出함

2010 年 12 月

高敏碩의 工學 碩士學位 論文을 認准함

審査委員長 鄭 釩 津 印

委 員 金 慶 淵 印

委 員 金 信 印

濟州大學校 大學院

2010 年 12 月

Determination of Void Fraction in Concentric Annular and Stratified Two Phase Flows Using Impedance Technique

Min Seok Ko

(Supervised by Professor Sin Kim)

A thesis submitted in partial fulfillment of the requirement
for the degree of Master of Engineering

2010. 12

This thesis has been examined and approved.

.....

Thesis director, Sin Kim, Prof. of Nuclear and Energy Engineering

.....

.....

.....

(Name and Signature)

.....

Date

Department of Nuclear and Energy Engineering

GRADUATE SCHOOL

JEJU NATIONAL UNIVERSITY

Contents

List of Figures

List of Tables

요 약

증기 발생기 세관 파단(Steam Generator Tube Rupture) 사고 시 파단 유량은 원자로 냉각재 계통의 감압, 증기 발생기 2차 측의 수위 및 압력 상승, 그리고 증기 발생기 주증기안전밸브(MSSV: Main Steam Safety Valve)의 개폐 등 주요 열수력 현상에 영향을 미치는 핵심 인자이다. 따라서 ATLAS(Advanced Thermal-hydraulic Test Loop for Accident Simulation)를 이용한 증기 발생기 세관 파단 사고모의 실험에서 계통의 열수력 현상을 상세하게 분석하기 위해 세관에서 방출되는 파단유량을 정밀하게 측정하는 것이 필수적이다. 본 연구는 파단유량 측정 기술개발을 위한 기초연구의 일환으로 환상 및 성층류 유동에서의 기포율 측정을 위한 표준 전기용량 혹은 저항과 기포율의 상관관계를 제안한다. 이 방법에서 표준 정전용량 혹은 저항은 기포율의 함수로 주어지게 되고 센서 크기 및 내부 물성치는 센서의 민감도를 결정하는 중요한 변수가 된다. 또한, 본 연구는 표준 정전용량 혹은 저항과 기포율의 상관관계를 아크릴 모형 장치(acrylic phantom)을 이용한 정상 상태 실험으로부터 검증하고 실제 적용을 위해 고려해야 되는 인자들에 대한 수치분석을 수행한다.

Summary

In case of STGR(Steam Generator Tube Rupture) break flow is one of the key parameters which have significant effects on thermal-hydraulic phenomena such as depressurization of the reactor coolant system, increase in water level and pressure in the secondary part of the steam generator and MSSV(Main Steam Safety Valve) switch of the steam generator, etc. Therefore, it is essential to precisely measure the break flow for accurate analysis of thermal-hydraulic phenomena in STGR simulation based on ATLAS. This study, as a preparatory research, proposes the relationship between the normalized capacitance or resistance and void fraction for the void fraction measurement in concentric annular flow and stratified flow in an effort to develop the break flow measurement technique. In proposed method the normalized capacitance or resistance is expressed as a function of the void fraction, and the sensor size as well as internal properties is a significant factor in determining the sensitivity of the sensor. This work also verifies the relationship between the normalized capacitance or resistance and void fraction by comparing with static phantom experiments, and performs the numerical analysis on considerations for real application of this method.

I. Introduction

Two-phase flow is a highly general phenomenon in various engineering systems including thermal-hydraulic systems of the nuclear power plant. In particular, the void fraction in two-phase system is one of the most significant parameters to be considered for efficient system design and analysis.

There have been various methods proposed for monitoring the void fraction. These void fraction monitoring techniques are mainly classified as either intrusive method or non-intrusive method. The intrusive method has an advantage in providing the local information such as the behavior of turbulent flow, however, it has a disadvantage of introducing flow disturbance at the same time. The non-intrusive methods such as radiation scattering, laser, ultrasound and NMR do not disturb the flow field. But, they are difficult to apply the case in which fast transients occur due to slow response time.

The Impedance method, on the other hand, has a number of desirable characteristics. In particular, the impedance method: (1) reduces the uncertainty of the experimental information since this method dose not disturb the flow field, (2) is possible to be applied to thermal-hydraulic system of the nuclear power plant which goes through fast transition due to sufficiently fast response to the void fraction, (3) is effective for large and small structures.

The electrical impedance method is based on the fact that the liquid and gas have different conductivity and permittivity values. In the electrical impedance method, the measured electrical impedance across an electrode pair is generally resistive when the frequency of the excitation signal is sufficiently high. For higher frequencies the behavior of the electrolyte tends to be capacitive. For this reason the impedance method is classified as either the resistance or

capacitance method according to the applied frequency. In the impedance method, resistive or capacitive response of two-phase field is measured for the injected current or applied voltage and then the resultant resistance or capacitance is used to directly estimate the void fraction as given in Fig. 1.

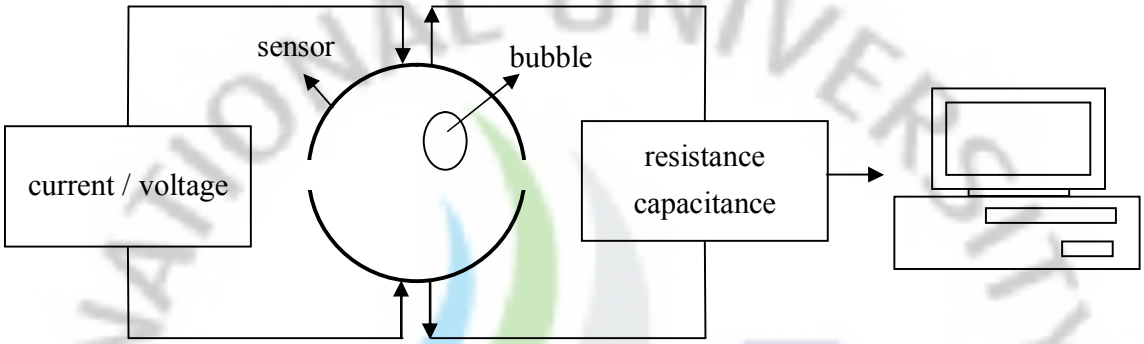

Figure 1: Conceptual diagram of the impedance method

Various designs of sensors for the impedance method have been proposed. Shu et al. (1982) suggested the curved plate-type sensor fitted to the outer wall of the pipe and derived an analytical relationship between the normalized capacitance and void fraction for concentric annular flow. Song et al. (1998) designed a conductance sensor flush-mounted to the inner wall of the pipe in order to measure the void fraction for bubbly and slug flow regimes in a vertical air-water flow. Davia and Fossa (2003) designed ring-type conductance sensor focusing on distance between sensors, which leads to different conductance signals. Zheng et al. (2008) proposed combination of turbine flowmeter and ring-type conductance sensor for gas-liquid two phase flow measurement.

II. Motivations and Coverage of this work

In case of SGTR (Steam Generator Tube Rupture) accident, the coolant in the primary system of the steam generator is released to the secondary system. In the early stage of the accident the single phase critical flow can occur due to the difference in pressure between the primary and secondary system of the reactor, however, as the pressure difference decreases this single phase critical flow is converted to water-steam two-phase flow. In SGTR accident break flow is one of the key parameters for thermal-hydraulic phenomena. Therefore, it is very important to precisely monitor break flow for the analysis of thermal-hydraulic phenomena and safety analysis.

In an effort to develop an impedance sensor for monitoring the void fraction of break flow in ATLAS (Advanced Thermal hydraulic Test Loop for Accident Simulation), which has been developed to investigate the thermal-hydraulic behavior for OPR1400 and APR1400, this work suggests theoretical relationship between the normalized capacitance or resistance and void fraction, and also deals with several considerations for the analysis of a capacitance signal in the sensor, for example, the effect of the temperature-dependent insulator and water on capacitance responses.

In the 3rd section, the theoretical relationship between the normalized capacitance or resistance and void fraction for concentric annular flow and stratified flow is proposed. This theoretical relationship is compared with static experiments in the 4th section. In the last section several factors to be considered for successful application of the capacitance sensor to real situations are taken care of.

III. Mathematical background

In the impedance method the phase distribution of two-phase flow is regarded as the distribution of electrical properties. Therefore, if electrical properties are once given, boundary voltage is determined by Maxwell equation with given boundary conditions:

$$\nabla \cdot \sigma \nabla u = 0, \tag{1}$$

where σ is the conductivity of the region of interest and u is the potential distribution to be determined. The resistance method uses the resistance response to the void fraction and this is accomplished by simply calculating the resistance on the sensor from Ohm's law.

In the capacitance method, on the other hand, boundary charge is calculated by the following Laplace equation with given boundary conditions:

$$\nabla \cdot \varepsilon \nabla u = 0, \tag{2}$$

where ε is the permittivity of the region of interest and u is the potential distribution to be determined. The capacitive method similarly focuses on the capacitance response to the void fraction and this is carried out by calculating the capacitance from the relationship between the charge and capacitance.

1. Concentric annular flow

(1) Capacitance method

Annular flow is a multiphase flow regime in which the lighter fluid flows into the center of the pipe, and the heavier fluid is contained in a thin film around the pipe wall. This occurs at high velocities of the lighter fluid. Figure 1 shows the schematic of concentric annular flow composed of water background and air. Their permittivity values are expressed as ε_w and ε_a, respectively, and they are assumed to be constant. Two identical sensors attached to the inner wall are located in the opposite side. The radius of the pipe is R_1 mm and the angle between sensors is 2δ. Voltages are applied to the left and right sensor with V_0 and $-V_0$, respectively.

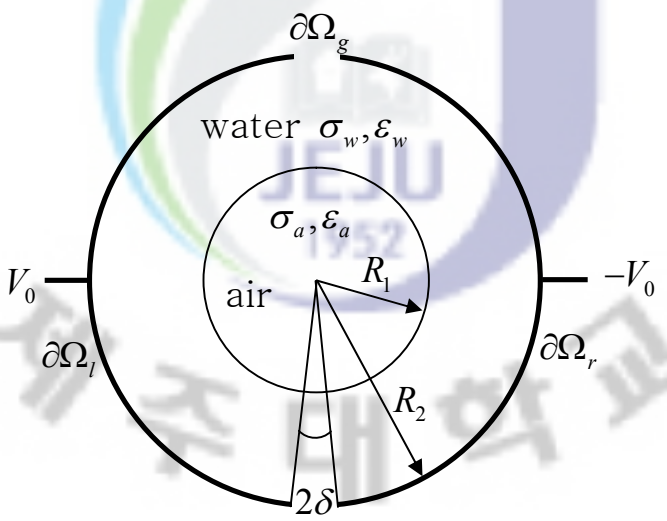

Figure 2: Schematic of concentric annular flow

In each region, the potential distribution satisfies the Laplace equation:

$$\nabla \cdot \varepsilon_w \nabla u_w = 0 \quad \text{for} \quad R_1 \le r \le R_2 \tag{3}$$

$$\nabla \cdot \varepsilon_a \nabla u_a = 0 \quad \text{for} \quad 0 \le r \le R_1 \tag{4}$$

where subscripts 'w' and 'a' denote the water and air region, respectively. The governing equations are subjected to the following boundary conditions:

$$V = V_0 \quad \text{on} \quad \partial\Omega_l \tag{5}$$

$$V = -V_0 \quad \text{on} \quad \partial\Omega_r \tag{6}$$

$$\varepsilon_w \frac{\partial u_w}{\partial r} = 0 \quad \text{on} \quad \partial\Omega_g \tag{7}$$

$$\varepsilon_w \left.\frac{\partial u_w}{\partial r}\right|_{r=R_1} = \varepsilon_a \left.\frac{\partial u_a}{\partial r}\right|_{r=R_1} \tag{8}$$

Here, $\partial\Omega_l$ and $\partial\Omega_r$ denote the left and right sensor, $\partial\Omega_g$ represents the gap between sensors. In Fig.2 or Eqs.(3) and (4), R_2 and R_1 are the radius of the sensor and air region. If the charge and voltage on the sensor are Q and V, then the capacitance C is $Q/\Delta V$, and here Q is evaluated from the charge density on the surface of the sensor. Now, we introduce the normalized capacitance C^*:

$$C^* = \frac{C - C_w}{C_a - C_w} \tag{9}$$

where C is the capacitance response to an arbitrary void fraction α which is defined as

$$\alpha = \left(\frac{R_1}{R_2} \right)^2 \tag{10}$$

C_a and C_w are the capacitance value for $\alpha = 1$ and $\alpha = 0$, respectively.

Kim et al. (2009) proposed analytical relationship between the normalized capacitance and void fraction with plate-type sensor attached to the inner wall of pipe. In that study, the normalized capacitance is expressed as a function of only void fraction for given relative permittivity and size of the sensor. That is, the normalize capacitance is given by

$$C^* = \frac{C - C_w}{C_a - C_w} = \frac{\sum_{n=odd}^{\infty} \frac{2\alpha^n}{(1+\lambda_c)+(1-\lambda_c)\alpha^n} \frac{\sin 2n\delta}{n^2}}{\sum_{n=odd}^{\infty} \frac{\sin 2n\delta}{n^2}} \tag{11}$$

where α is the void fraction given as Eq.(10) and λ_c is the ratio of the permittivity or the capacitance, that is,

$$\lambda_c = \frac{\varepsilon_a}{\varepsilon_w} = \frac{C_a}{C_w} \tag{12}$$

This ratio is experimentally obtained. That is, the ratio of capacitance measurement for $\alpha = 1$ to $\alpha = 0$ is used as λ_c since the capacitance is directly proportional to the relative permittivity as given in Eq.(12). Therefore, it is very important to obtain accurate reference capacitances for the estimation of the void fraction based on the normalized capacitance.

(2) Resistance method

In the same manner as the capacitance method, the domain consists of two regions, the air and water as shown in Fig.2. Their conductivity values are expressed as σ_a and σ_w, they are also assumed to be constant. The potential distribution in each region satisfies the Maxwell equation:

$$\nabla \cdot \sigma_w \nabla u_w = 0 \quad \text{for} \quad R_1 \le r \le R_2 \tag{13}$$

$$\nabla \cdot \sigma_a \nabla u_a = 0 \quad \text{for} \quad 0 \le r \le R_1 \tag{14}$$

The governing equations are subjected to the following boundary conditions:

$$V = V_0 \quad \text{on} \quad \partial\Omega_l \tag{15}$$

$$V = -V_0 \quad \text{on} \quad \partial\Omega_r \tag{16}$$

$$\sigma_w \frac{\partial u_w}{\partial r} = 0 \quad \text{on} \quad \partial\Omega_g \tag{17}$$

$$\sigma_w \left.\frac{\partial u_w}{\partial r}\right|_{r=R_1} = \sigma_a \left.\frac{\partial u_a}{\partial r}\right|_{r=R_1} \tag{18}$$

If the current and voltage on the sensor are I and V, then the resistance R is $\Delta V / I$, and here I is evaluated from the current density on the surface of the sensor. Now, we introduce the normalized resistance R^*:

$$R^* = \frac{R_w}{R} \tag{19}$$

where R is the resistance response to the void fraction which is defined as Eq. (16) and R_w is the resistance value for $\alpha = 0$.

Due to the similarity between the governing equation and boundary conditions of these two methods, the analytical relationship given as Eq. (11) can be simply extended to the resistance method. That is, if the conductivity of the air and water and the angle between sensors are σ_a, σ_w and 2δ as shown in Fig. 2, then the relationship between the normalized resistance and void fraction for the case of concentric annular flow can be expressed as

$$R^* = \frac{R_w}{R} = 1 - \frac{\sum_{n=odd}^{\infty} \frac{2(1-\lambda_r)\alpha^n}{(1+\lambda_r)+(1-\lambda_r)\alpha^n} \frac{\sin 2n\delta}{n^2}}{\sum_{n=odd}^{\infty} \frac{\sin 2n\delta}{n^2}} \tag{20}$$

here, λ_r is the ratio of the air conductivity to water conductivity or the resistance, that is,

$$\lambda_r = \frac{\sigma_a}{\sigma_w} = \frac{R_w}{R_a} \tag{21}$$

Since the ratio λ_r is close to zero for air-water two phase system Eq. (20) is simplified as

$$R^* = \frac{R_w}{R} = 1 - \frac{\sum_{n=odd}^{\infty} \frac{2\alpha^n}{1+\alpha^n} \frac{\sin 2n\delta}{n^2}}{\sum_{n=odd}^{\infty} \frac{\sin 2n\delta}{n^2}} \tag{22}$$

From Eq.(22) it is seen that the normalized resistance is expressed as a function of the void fraction for given half angle between sensors. However, it should be noted that Eq.(22) is only valid for air-water two phase flow. For other two phase flow systems Eq.(20) is recommended.

2. Stratified flow

Stratified flow is a multiphase regime in the horizontal pipe in which the fluids are separated into different layers, with lighter fluids flowing above heavier fluids. The stratified flow generally occurs at low flow rates. Figure 3 shows the schematic of stratified flow.

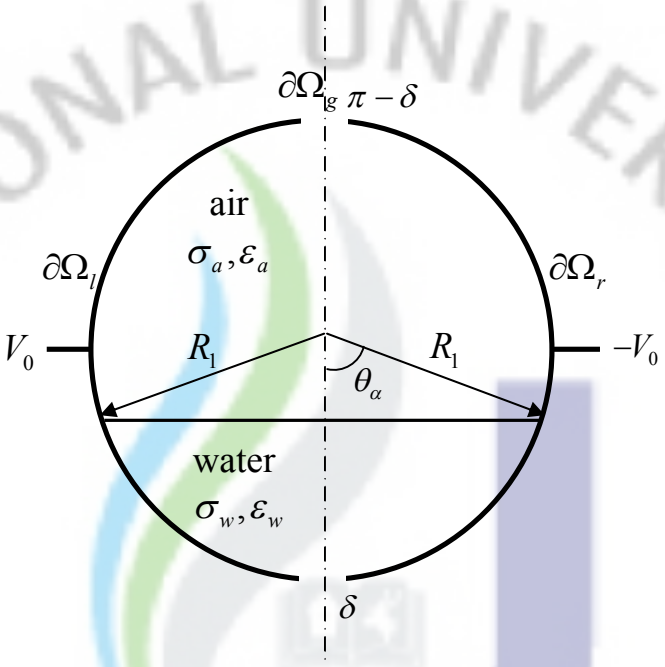

Figure 3: Schematic of stratified flow

The potential distribution in each region satisfies the Laplace equation given in Eqs. (3) and (4) or (13) and (14), and also these governing equations are subjected to Eqs. (5) ~ (8) or (15) ~ (18) in the same manner as concentric annular flow. However, resistive or capacitive responses for different expression of the void fraction which is given as Eq. (23) are calculated.

$$\alpha = 1 - \frac{\theta_\alpha - \sin\theta_\alpha \cos\theta_\alpha}{\pi} \tag{23}$$

where θ_α is the angle created by the radius of the pipe and water level.

For stratified flow the lack of axial symmetry of two phases makes it difficult to derive the analytical solution of the Laplace equation. Shu et al.(1982) and Wael H. Ahmed (2006) adopted the concept of simple equivalent circuit to analyze this problem. In this method two phases are regarded as series or parallel capacitors. That is, if the total differential capacitance is dC and the differential capacitance of water and air region are dC_w and dC_a, the total differential capacitance is given by

$$dC = dC_w + dC_a \tag{24}$$

where

$$dC_w = \varepsilon_w L \frac{d\theta}{2\sin\theta}, \quad \delta \le \theta \le \theta_\alpha \tag{25}$$

$$dC_a = \varepsilon_a L \frac{d\theta}{2\sin\theta}, \quad \theta_\alpha \le \theta \le \pi - \delta \tag{26}$$

Integrating Eqs. (24) over θ from δ to $\pi - \delta$, we have

$$C = \frac{\varepsilon_w L}{2} \ln\left[\frac{\tan(\theta_\alpha / 2)}{\tan(\delta / 2)}\right] + \frac{\varepsilon_a L}{2} \ln\left[\frac{\tan(\pi - \delta / 2)}{\tan(\theta_\alpha / 2)}\right] \tag{27}$$

Since $\theta_\alpha = \pi - \delta$ at $\alpha = 0$ and $\theta_\alpha = \delta$ at $\alpha = 1$, we have

$$C_w = -\varepsilon_w L \ln\left[\tan\left(\delta / 2\right)\right] \tag{28}$$

and

$$C_a = -\varepsilon_a L \ln\left[\tan\left(\delta / 2\right)\right] \tag{29}$$

Therefore, the normalized capacitance becomes

$$C^* = \frac{C - C_w}{C_a - C_w} = \frac{\left\{ \ln\left[\frac{\tan(\theta_\alpha / 2)}{\tan(\delta / 2)} \right] + 2\ln\left[\tan\left(\delta / 2\right) \right] \right\} + \lambda_c \ln\left[\frac{\tan(\pi - \delta / 2)}{\tan(\theta_\alpha / 2)} \right]}{2\left(1 - \lambda_c\right)\ln\left[\tan\left(\delta / 2\right) \right]} \tag{30}$$

Applying this concept to the resistance method we have the normalized resistance:

$$R^* = \frac{R_w}{R_T} = -\frac{\ln\left[\frac{\tan(\theta_\alpha / 2)}{\tan(\delta / 2)} \right]}{2\ln\left[\tan(\delta / 2) \right]} \tag{31}$$

where λ_c is the ratio of the air to water permittivity. Figure 4 and 5 show the relationship between the normalized capacitance or resistance and void fraction for $\delta = 0.025$ based on Eqs.(30), (31) and numerical calculation.

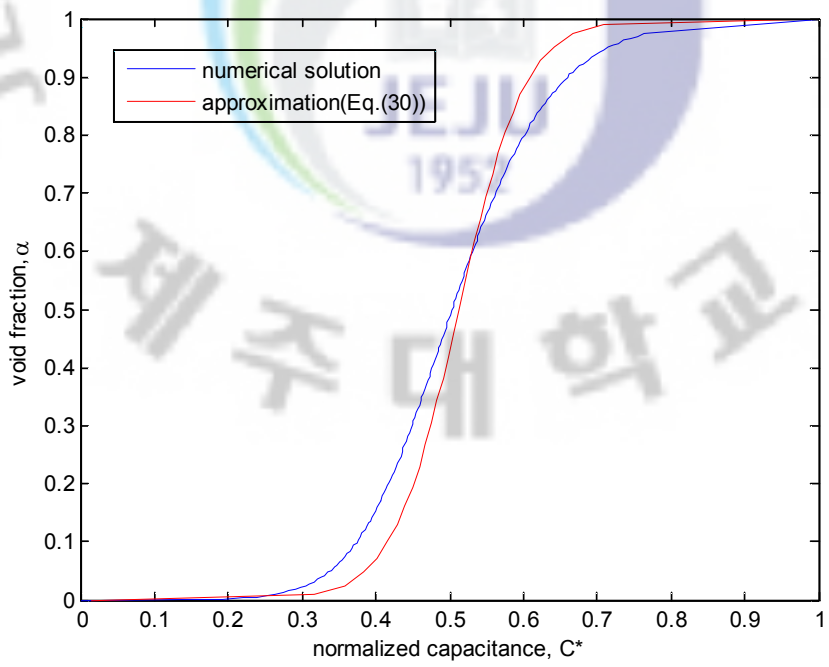

Figure 4: Comparison of the normalized capacitance-void fraction relationship between numerical calculation and approximate formula

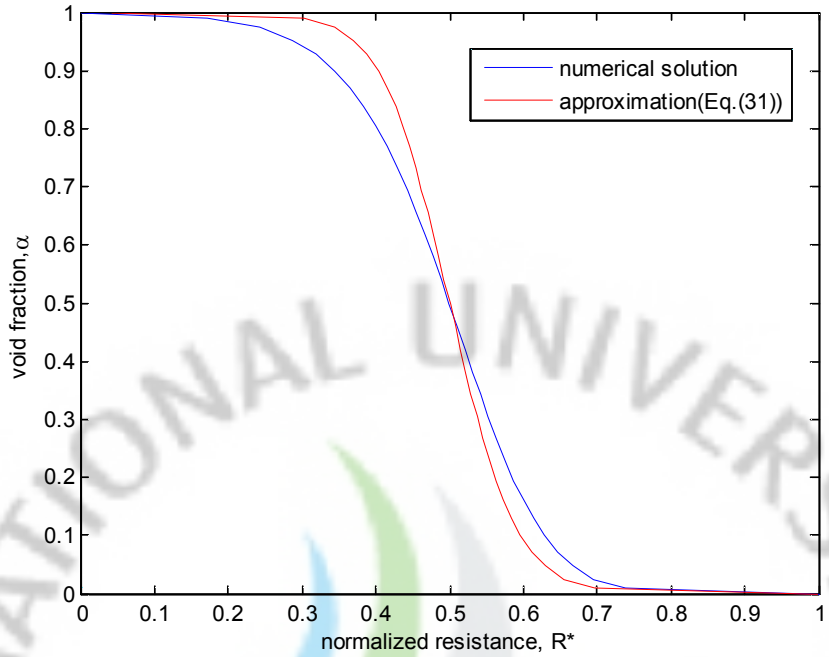

Figure 5: Comparison of the normalized resistance-void fraction relationship between numerical calculation and approximate formula

It should be noted that this simple model which is based on one-dimensional equivalent circuit cannot give exact results but just provide approximate trend of the normalized capacitance or resistance for the void fraction. Therefore, this study deals with stratified flow problem using a numerical method.

IV. Determination of the size of the sensor

For both concentric annular and stratified flow, the potential distributions are evaluated by COMSOL Multiphysics which is based on the finite element method. From the solutions of the Laplace equations the resistive and capacitive responses to variations of the void fraction are assessed as mentioned in the previous section.

In order to find the optimal size of the sensors, a number of simulations have been performed with respect to the angle between sensors, that is, $\delta = 1.4^{\circ}$, 2.8°, 4.2°, 5.6°, and 7.0°. The applied voltages used for simulations are 1 for the left sensor and -1 for the right sensor, and commonly used conductivity and permittivity values are used to define each region as given in Table1.

Table 1: Electrical properties used for simulations

Electrical properties	Air region	Water region
Relative permittivity, ε_r	1	80
Conductivity, σ (S/cm)	10e-10	0.0005

Figures 6 and 7 show the relationship between the normalized capacitance or resistance and void fraction with respect to the angle between sensors for concentric annular flow.

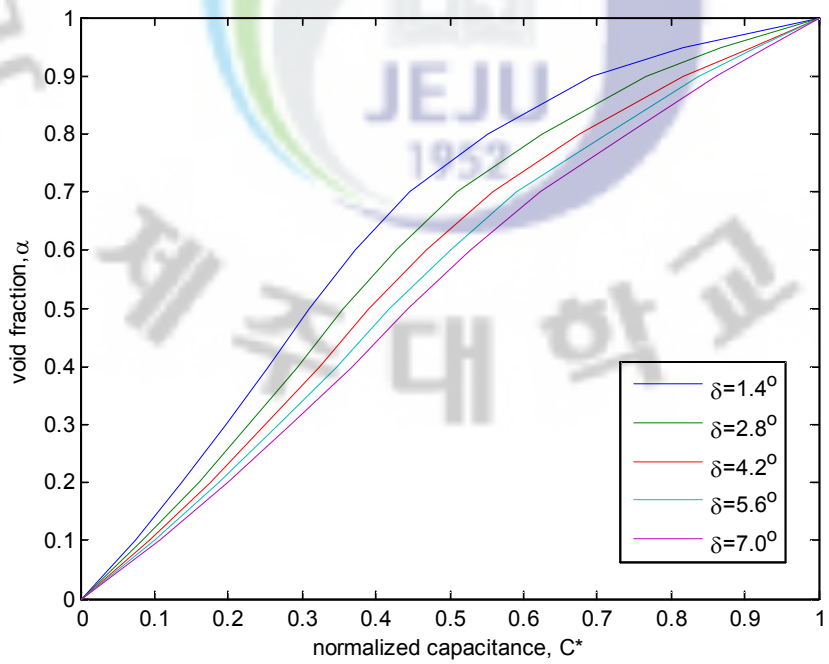

Figure 6: Capacitance response to the void fraction with respect to the angle between sensors for concentric annular flow

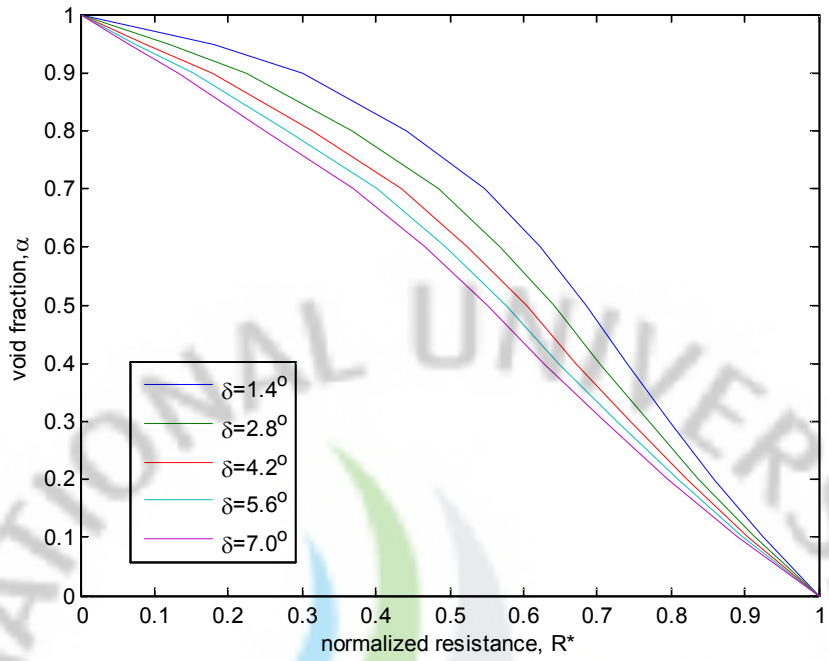

Figure 7: Resistance response to the void fraction with respect to the angle between sensors for concentric annular flow

According to Figs.6 and 7, the relationship between the normalized capacitance or resistance and void fraction becomes linear as the angle between sensors increase, on the contrary, the decrease in the angle causes the sensitivity of the sensor to be higher for high void fraction region. For the quantitative evaluation of the effect of the sensor size, we introduce the sensitivity:

$$\text{Sensitivity} = \frac{\Delta C^*}{\Delta \alpha} \tag{32}$$

and

$$\text{Sensitivity} = \frac{\Delta R^*}{\Delta \alpha} \tag{33}$$

Table 2 shows the sensitivity of the sensors for given void fraction regions in concentric annular flow.

Table 2: Sensitivity of the sensors for concentric annular flow

Half angle between sensors(δ)	1.4°	2.8°	4.2°	5.6°	7.0°
Capacitance method:					
$\alpha \le 0.3$	0.197	0.227	0.251	0.268	0.285
$0.3 \le \alpha \le 0.7$	0.249	0.283	0.309	0.324	0.338
$\alpha \ge 0.7$	0.449	0.373	0.323	0.288	0.260
Resistance method:					
$\alpha \le 0.3$	0.199	0.229	0.252	0.270	0.287
$0.3 \le \alpha \le 0.7$	0.249	0.283	0.309	0.324	0.338
$\alpha \ge 0.7$	0.552	0.488	0.439	0.406	0.375

From Figs 6, 7 and Table 2, for both methods the smaller angle between sensors is more advantageous in monitoring the void fraction above 0.7. For the void fraction below 0.3, on the other hand, the bigger angle between sensors is more competitive. Since the void fraction is generally above 0.8 in annular flow, the smaller angle is recommended, that is, $\delta = 1.4^{\circ}$.

Similarly, for stratified flow several simulations are carried out to demonstrate the relationship between the void fraction and normalized capacitance or resistance with respect to the size of the sensor. The same electrical properties and angle between sensors which are adopted for simulations of concentric annular flow are considered.

Figures 8 and 9 show the relationship between the normalized capacitance or resistance and void fraction for stratified flow.

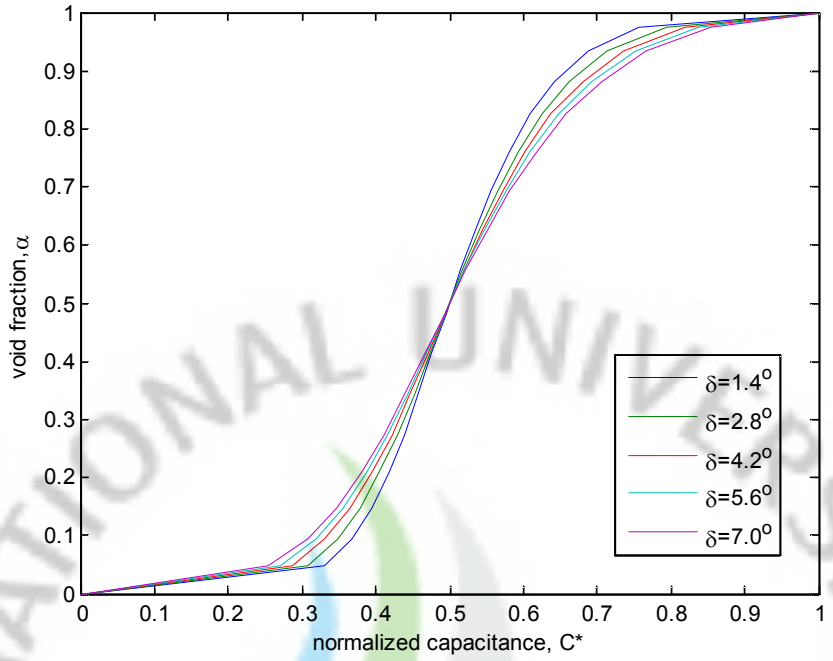

Figure 8: Capacitance response to the void fraction with respect to the angle between sensors for stratified flow

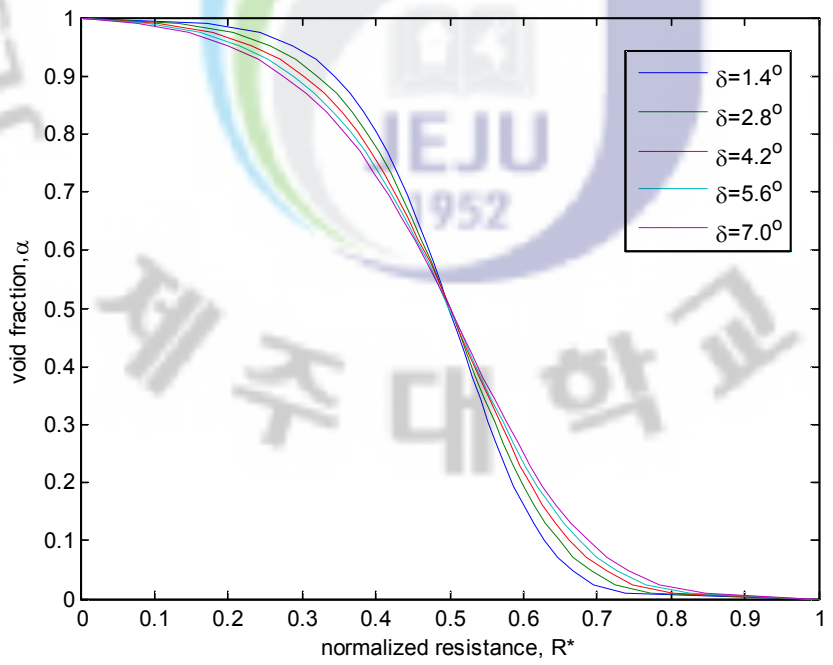

Figure 9: Resistance response to the void fraction with respect to the angle between sensors for stratified flow

We also introduce the sensitivity of the sensors with respect to the angle between sensors for both methods using Eqs.(32) and (33).

Table 3: Sensitivity of the sensors for the stratified flow

Half angle between sensors(δ)	1.4°	2.8°	4.2°	5.6°	7.0°
Capacitance method:					
$\alpha \le 0.3$	0.449	0.442	0.436	0.431	0.426
$0.3 \le \alpha \le 0.7$	0.121	0.138	0.153	0.164	0.175
$\alpha \ge 0.7$	0.430	0.420	0.411	0.405	0.398
Resistance method:					
$\alpha \le 0.3$	0.447	0.439	0.433	0.428	0.423
$0.3 \le \alpha \le 0.7$	0.110	0.126	0.140	0.150	0.160
$\alpha \ge 0.7$	0.443	0.435	0.427	0.422	0.417

According to Figs. 8, 9 and Table 3, for both methods the smaller angle between sensors is slightly more advantageous in determining the void fraction above 0.7 and below 0.3. However, for the void fraction region between 0.3 and 0.7 adopting bigger sensor is more reasonable way. In short, if the high void fraction is dominant in the system, the bigger sensor is more reliable for determining the void fraction based on the normalized capacitance or resistance regardless of flow patterns. On the other hand, if the low void fraction is of interest, the smaller sensor is more realistic.

V. Experiment and Result

For the verification of this method to estimate the void fraction based on the normalized capacitance or resistance, several experiments with a static phantom have been performed. A cylindrical acryl pipe of inner radius 40 mm is employed for experiments. Two stainless steel sensors are attached to the inner wall of the pipe. The height of sensors is 40 mm. The gap between sensors is 2 mm ($\delta = 1.4^{\circ}$) and this gap is electrically insulated. The reference capacitances in Eq. (9), that is, C_a and C_w, are measured by using an acryl rod with 40 mm radius and by using the pipe filled with water only. For concentric annular flow, ten acryl rods are designed to describe the void fraction of 0.1, 0.2, …, 0.9 and 0.95 as given in Fig. 10. The capacitances are measured with the Agilent 4284A LCR meter. The signal frequencies of the LCR meter are 1000 kHz for both capacitance and resistance method. The applied voltage is 1 V for both methods. The sensors are connected to the LCR meter with 1m long dedicated shield cables, Agilent 16089B Kelvin Clip Leads. Table 2 summarizes experimental setup and conditions.

Table 4: Specifications of sensor and experimental conditions

	Capacitive or resistive method
Radius of the pipe	40mm
Number of sensors	2
Height of sensors	40mm
Angle between sensors	1.4°
Signal frequency	1000 kHz
Input voltage	1V
Operating temperature	20℃

For stratified flow, static experiments have been carried out by simply holding the sensors horizontally and by adding a measured volume of the water under the same experimental conditions as the case of concentric annular flow. Figures 11 and 12 show a photograph of the cylindrical acryl pipe with two stainless steel sensors for concentric annular and stratified flow.

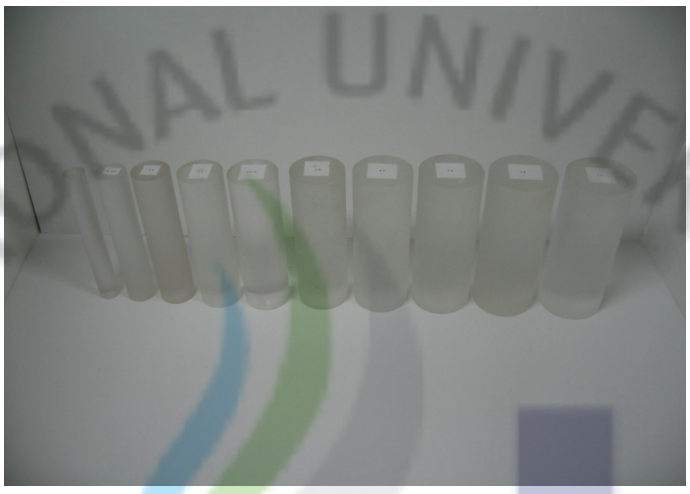

Figure 10: Acryl rods for description of void fractions

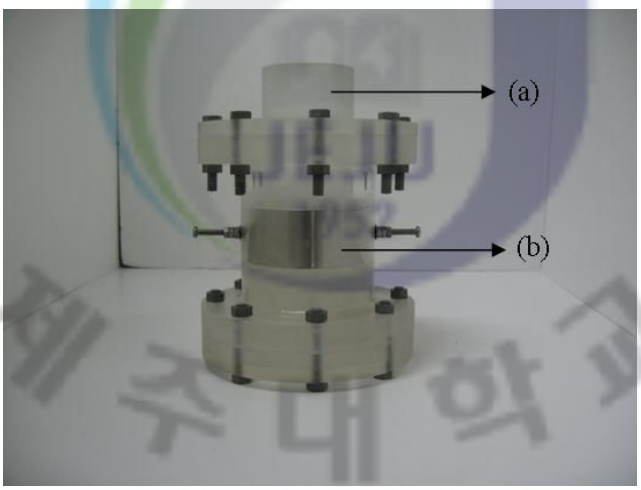

Figure 11: Sensor for static experiments of concentric annular flow. (a) acryl rod; (b) sensor

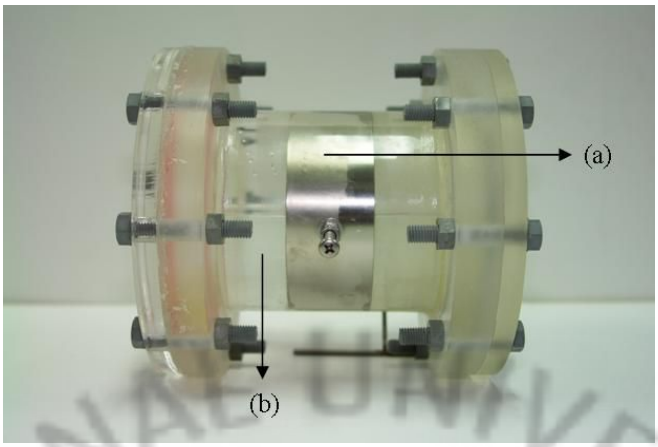

Figure 12: Phantom for static experiments of stratified flow. (a) sensor; (b) water

For the static experiments of concentric annular flow, a flange has been designed to locate acryl rods in the exact center so that any unnecessary errors do not occur. In the static experiments of each case, annular and stratified type, 100 measurements are repeated for the given void fractions. The measured capacitances range from 7.0 pF ($\alpha = 1$) to 127.5 pF ($\alpha = 0$), and their standard deviations are less than 0.05%. In the case of resistance method, the measured resistance ranges from 622Ω ($\alpha = 0$) to 2445Ω ($\alpha = 0.95$), and their standard deviations are below 0.07%. Figures 13,14,15 and 16 show the comparison between theoretical and experimental results.

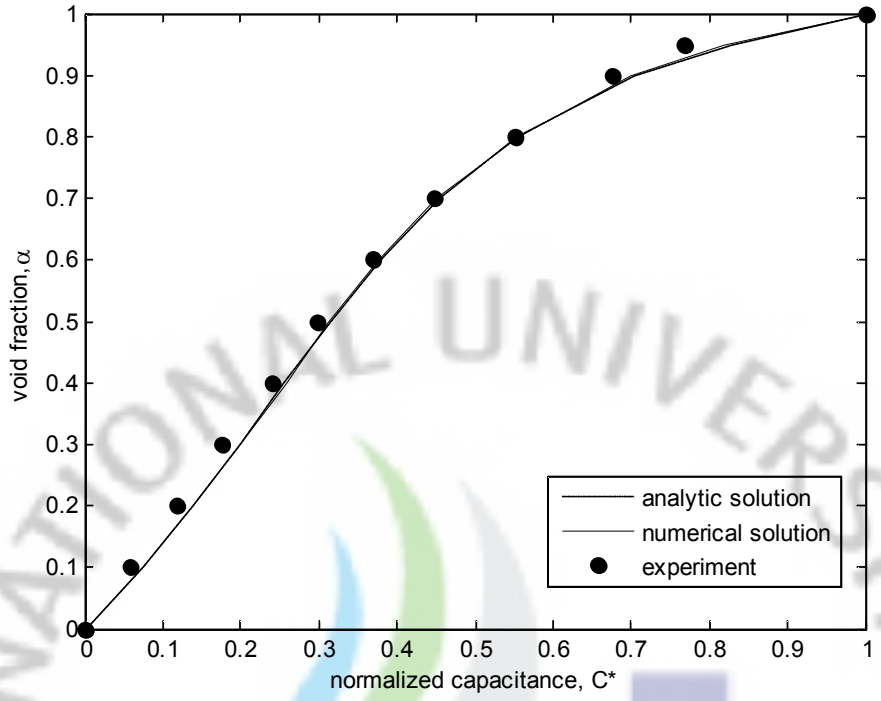

Figure 13: Capacitance response to void fractions for concentric annular flow at 1MHz

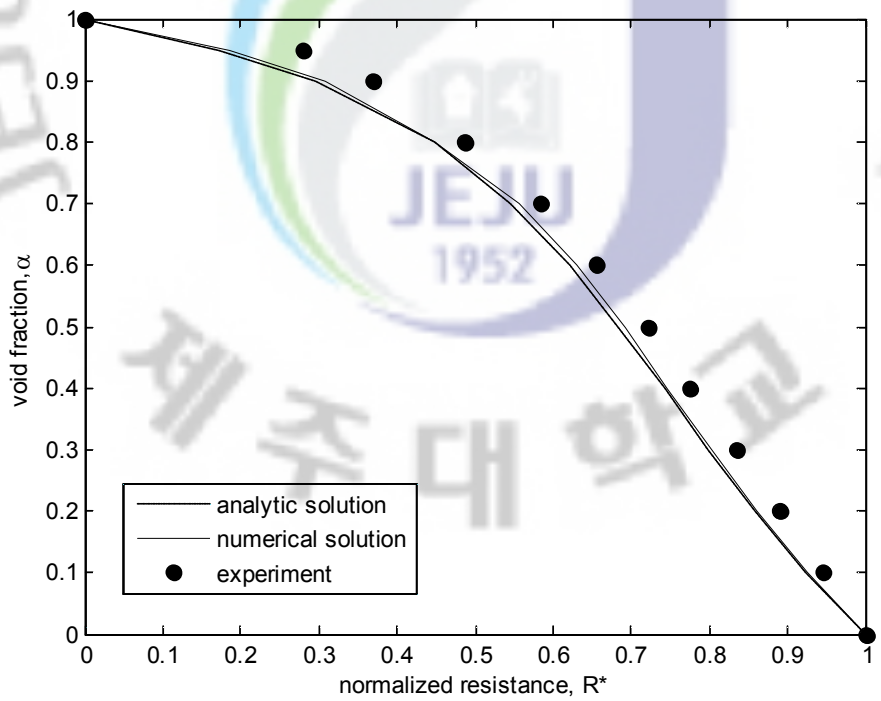

Figure 14: Resistance response to void fractions for concentric annular flow at 1MHz

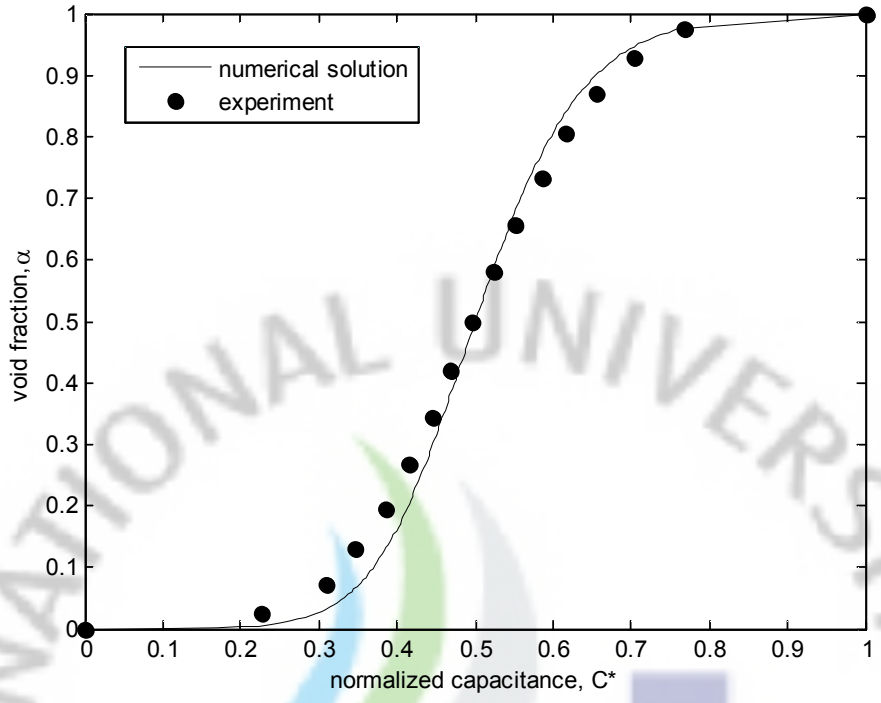

Figure 15: Capacitance response to void fractions for stratified flow at 1MHz

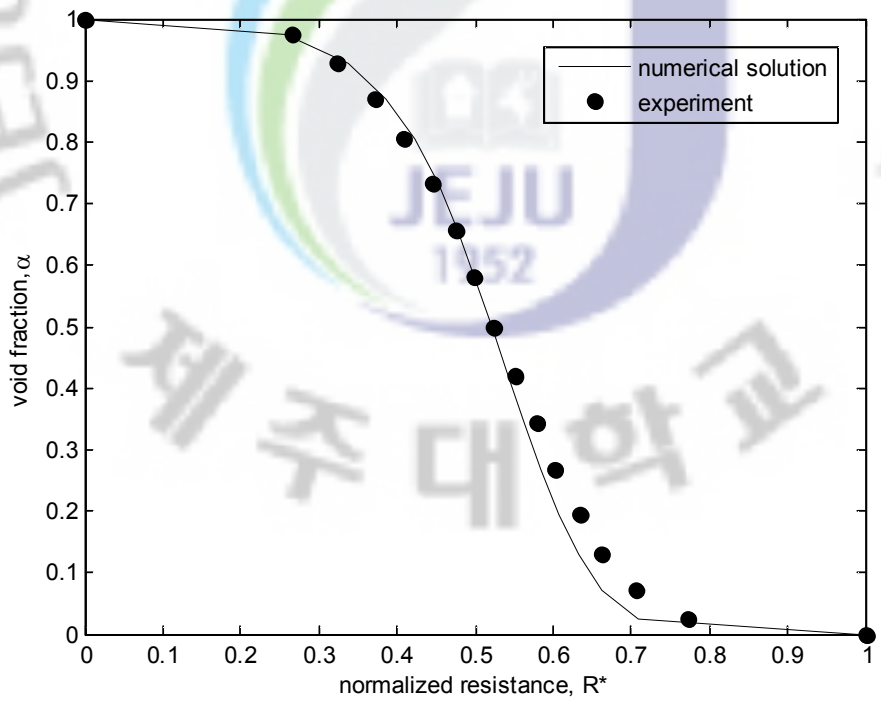

Figure 16: Resistance response to void fractions for stratified flow at 1MHz

The comparison results show that experimental results approximately match the predicted behavior. For the performance evaluation of the theoretical relationship and the sensor we introduce the error as follows:

$$\text{Err} = \sqrt{\frac{\sum\left(C^*_{\text{theory}} - C^*_{\text{exp}}\right)^2}{\sum\left(C^*_{\text{theory}}\right)^2}} \quad \text{or} \quad \text{Err} = \sqrt{\frac{\sum\left(R^*_{\text{theory}} - R^*_{\text{exp}}\right)^2}{\sum\left(R^*_{\text{theory}}\right)^2}} \tag{34}$$

where C^*_{theory} and C^*_{exp} are theoretical and experimental normalized capacitance value for given void fractions. Similarly, R^*_{theory} and R^*_{exp} are theoretical and experimental normalized resistance value. According to Table 5, maximum error between the theoretical relationship and experimental results is approximately 14%, and this occurs in concentric annular flow. This error is thought to be caused by not considering the effect of contact impedance in the theoretical relationship as well as small mismatch of the sensor size or gap between sensors. The contact impedance is a small resistive component which occurs at the interface between the surface of the sensor and fluid. This is mainly affected by the condition of the sensor and electrical properties of the fluid. Therefore, sophisticated fabrication is essential along with consideration of contact impedance for the impedance method.

Table 5: Performance evaluation of the sensor and theoretical relationship

Flow pattern	Error
Concentric annular flow:	
Capacitance method	
$\alpha \leq 0.3$	0.135
$0.3 \leq \alpha \leq 0.7$	0.043
$\alpha \geq 0.7$	0.042
Resistance method	
$\alpha \leq 0.3$	0.027
$0.3 \leq \alpha \leq 0.7$	0.045
$\alpha \geq 0.7$	0.143
Stratified flow:	
Capacitance method	
$\alpha \leq 0.27$	0.110
$0.27 \leq \alpha \leq 0.73$	0.016
$\alpha \geq 0.73$	0.016
Resistance method	
$\alpha \leq 0.27$	0.051
$0.27 \leq \alpha \leq 0.73$	0.020
$\alpha \geq 0.73$	0.032

VI. Considerations for real application of capacitance sensor

1. Capacitance sensor for void fraction measurement of break flow in ATLAS

In ATLAS experiment such as LOCA, break flow is separated into the water and steam in separator and then these water and steam flow are indirectly measured by using an electronic scale and a vortex flowmeter. However, break flow in SGTR can not be measured in the indirect way since the coolant of primary system is released to the secondary system. KAERI proposed a direct method to measure break flow in STGR simulation. The basic idea of the method is to convert the void fraction of the system which is measured by CVM(Capacitance Void Meter) into break flow of two phase flow. For this, KAERI designed a capacitance sensor as shown in Fig. 16. Two sensors are attached in the inner wall of the insulator which is made from zirconium dioxide (ZrO_2). The radius of the inner pipe is 10.6mm and that of insulator is 22.5mm. The gap between sensors is 2mm ($\approx 5.4°$) and the thickness of the sensors is also 2mm. This module consisting of sensors and ceramic insulator is inserted into pipeline of ATLAS for void fraction measurement.

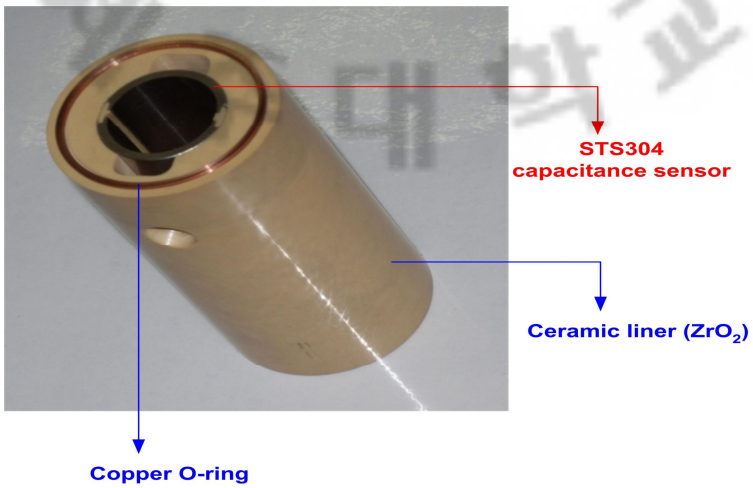

Figure 17: Capacitance sensor for void fraction measurement of break flow in ATLAS

2. Considerations for analysis of sensor signal for void fraction measurement

The accurate assessment of the void fraction is an extremely significant issue to successfully apply the direct measurement method for break flow to ATLAS simulations. As a preparatory research this section takes care of several considerations which can be very important for the analysis of the sensor response to the void fraction. These are mainly classified in three parts:

① Effect of insulator on capacitance signal

② Effect of temperature-dependent insulator on capacitance signal

③ Effect of temperature-dependent permittivity of water on capacitance signal

The effect of the insulator on capacitance response is assessed by simply comparing with the case that no insulator is installed in the sensor module. This is handled in section (1). In section (2), different permittivity values of insulator are used to describe the effect of temperature-dependent insulator assuming constant permittivity values of water and air. Similarly, in section (3) various permittivity values of water are used to evaluate the effect of temperature-dependent permittivity of the water on capacitance signal by fixing the relative permittivity of insulator and by assuming that the air is not dependent on temperature.

(1) Effect of insulator on capacitance signal

Figure 18 shows the geometric arrangement of the domain which is based on Fig. 17. The domain consists of water-air two phase region inside two sensors fitted to the inner wall of the insulator.

The voltages, V_0 and $-V_0$ are applied to the outer boundary of the sensors. The zero charge condition for capacitance method or insulation condition for resistance method is imposed on the outmost boundary and continuity condition is applied to the remaining boundaries. These conditions are given as Eqs. (5), (6), (7), (8), (17) and (18).

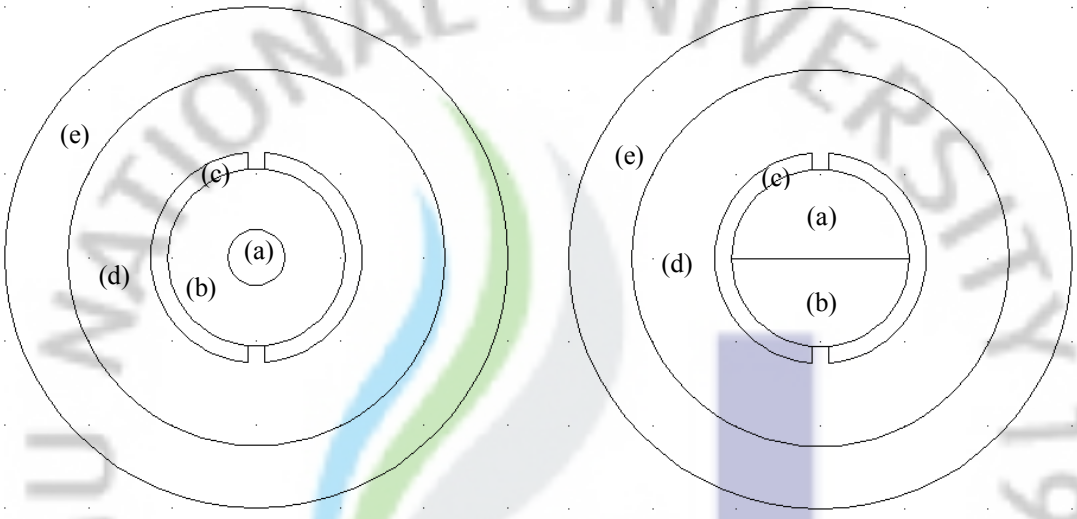

Concentric annular flow Stratified flow

Figure 18: Geometry for simulations. (a) air; (b) water; (c) sensor; (d) ceramic insulator; (e) outer pipe

Since the relative permittivity of the conductor tends to be infinite, sufficiently high relative permittivity value, that is, 10^{10} is used for the stainless steel sensor and pipe. The relative permittivity of zirconia (ZrO_2) has been known as 12 at room temperature and 1MHz. Therefore, this value is used to define the ceramic insulator. Table 6 shows the relative permittivity used to define each component for simulations. For the assessment of the effect of the insulator on capacitance signal, the capacitance response which is calculated in the real

geometry given as Figs. 17 or 18, is compared with the case in which no insulator is involved (See Figs. 2 and 3).

Table 6: Relative permittivity used for simulations

Components	Relative permittivity, ε_r
Stainless steel pipe	10^{10}
Stainless steel sensors	10^{10}
Ceramic insulator	12
Water	80
air	1

Figures 19 and 20 show the simulation results for concentric annular and stratified flow, respectively. In these figures, red line represents the normalized capacitance-void fraction relationship based on real geometry and blue line denotes the case in which the insulator is not considered. The maximum error between these two cases is roughly 4.5% for concentric annular flow. In case of stratified flow the maximum error is approximately 6.5% and this occurs at low void fraction region. This implies that the effect of the insulator may be considered for accurate analysis.

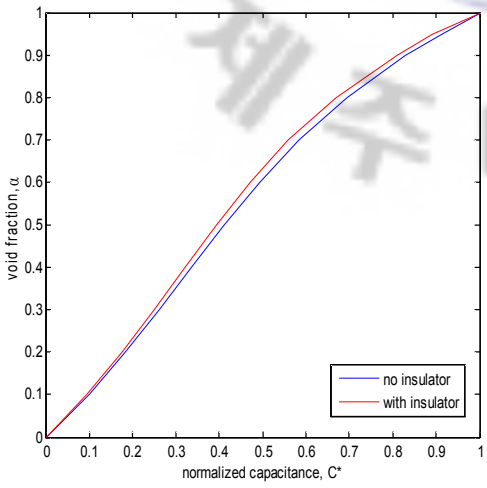

Void fraction, α	$\left\lvert \frac{C^*_{\text{no insulator}} - C^*_{\text{with insulator}}}{C^*_{\text{no insulator}}} \right\rvert$
0.1	0.0436
0.2	0.0375
0.3	0.0432
0.4	0.0438
0.5	0.0431
0.6	0.0447
0.7	0.0443
0.8	0.0366
0.9	0.0223

Figure 19: Effect of insulator on capacitance signal for concentric annular flow

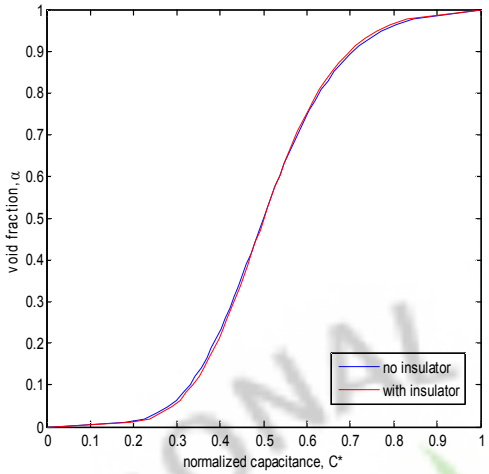

Void fraction, α	$\left\lvert \frac{C^*_{\text{no insulator}} - C^*_{\text{with insulator}}}{C^*_{\text{no insulator}}} \right\rvert$
0.1	0.0228
0.2	0.0165
0.3	0.0076
0.4	0.0056
0.5	0.0017
0.6	0.0008
0.7	0.0047
0.8	0.0072
0.9	0.0110

Figure 20: Effect of insulator on capacitance signal for stratified flow

(2) Effect of the temperature-dependent insulator on capacitance signal

As a practical matter, ceramic materials that satisfy the following property criteria at 25℃ is classified as good insulators:

- Dielectric constant (relative permittivity), $\varepsilon_r \leq 30$
- Electrical resistivity, $\rho \geq 10^{12}\ (\Omega \cdot cm)$

The relative permittivity of most ceramic insulators range from 5 to 15 and their resistivity values are commonly over $10^{12}\ (\Omega \cdot cm)$ at 25℃ and 1MHz. These electrical properties are dependent on temperature, that is, relative permittivity and electrical conductivity of insulators tend to increase with temperature. This is largely due to contents and properties of additives. For example, the relative permittivity value of zircon porcelain is roughly 10 at room temperature and slightly changes with temperature, $\varepsilon_r = 15$ at 300℃. On the other hand, in case of steatite its relative permittivity is constant up to around 300℃ and then sharply increases with temperature.

The research on temperature-dependent electrical properties of zirconia (ZrO_2) which is used for insulator of capacitance sensor module has not been widespread. Therefore, this work assumes that relative permittivity value of zirconia insulator changes from 12 (room temperature) to 30 which is typical criteria for insulator for given permittivity values of water and air, that is, $\varepsilon_a / \varepsilon_w = 0.0125,\ 0.05,\ 0.1,$ and 0.2.

Figures 21~28 show the capacitance response to void fraction for various permittivity values of the insulator, ε_z.

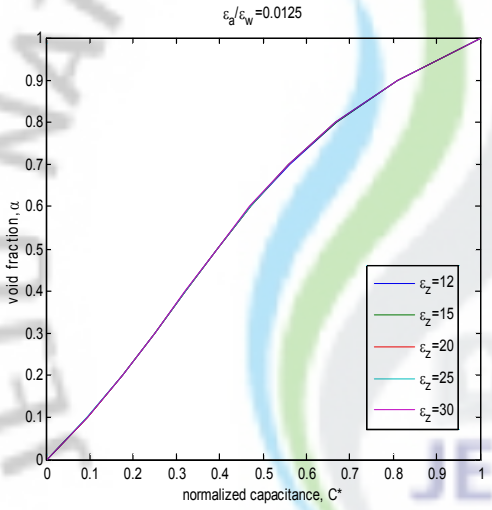

Void fraction, α	$\left\lvert \frac{C^*_{\varepsilon_z=12} - C^*_{\varepsilon_z=30}}{C^*_{\varepsilon_z=12}} \right\rvert$
0.1	0.0021
0.2	0.0029
0.3	0.0047
0.4	0.0039
0.5	0.0033
0.6	0.0036
0.7	0.0033
0.8	0.0023
0.9	0.0002

Figure 21: Effect of temperature-dependent insulator on capacitance signal for $\varepsilon_a / \varepsilon_w = 0.0125$ in concentric annular flow

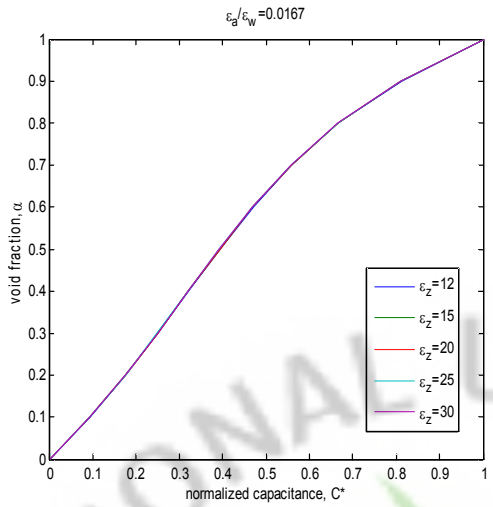

Void fraction, α	$\left\|\frac{C^*_{\varepsilon_z=12}-C^*_{\varepsilon_z=30}}{C^*_{\varepsilon_z=12}}\right\|$
0.1	0.0020
0.2	0.0036
0.3	0.0041
0.4	0.0068
0.5	0.0046
0.6	0.0047
0.7	0.0041
0.8	0.0037
0.9	0.0011

Figure 22: Effect of temperature-dependent insulator on capacitance signal for $\varepsilon_a / \varepsilon_w = 0.0167$ in concentric annular flow

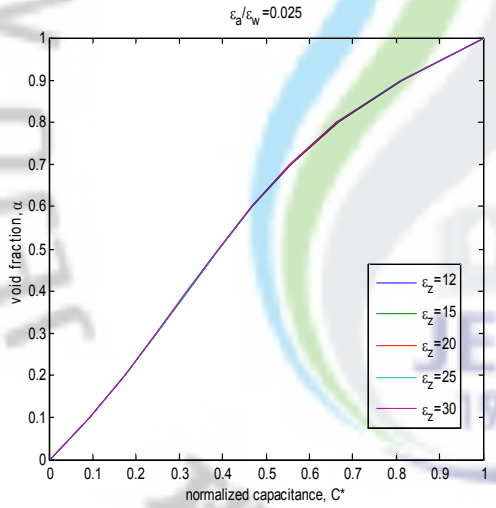

Void fraction, α	$\left\|\frac{C^*_{\varepsilon_z=12}-C^*_{\varepsilon_z=30}}{C^*_{\varepsilon_z=12}}\right\|$
0.1	0.0081
0.2	0.0069
0.3	0.0089
0.4	0.0063
0.5	0.0062
0.6	0.0074
0.7	0.006
0.8	0.0042
0.9	0.0007

Figure 23: Effect of temperature-dependent insulator on capacitance signal for $\varepsilon_a / \varepsilon_w = 0.025$ in concentric annular flow

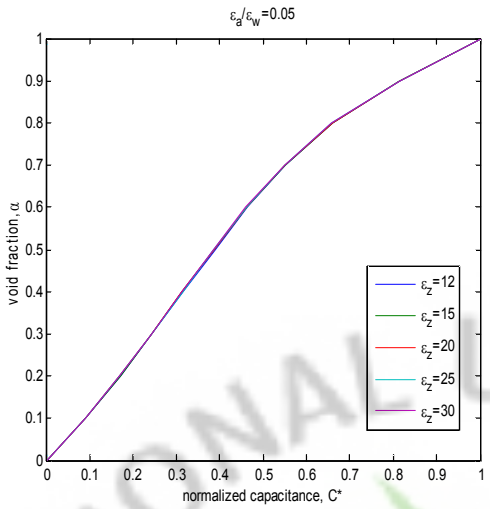

Void fraction, α	$\left\|\frac{C^*_{\varepsilon_z=12} - C^*_{\varepsilon_z=30}}{C^*_{\varepsilon_z=12}}\right\|$
0.1	0.0083
0.2	0.0076
0.3	0.0074
0.4	0.0073
0.5	0.0103
0.6	0.0072
0.7	0.0050
0.8	0.0053
0.9	0.0004

Figure 24: Effect of temperature-dependent insulator on capacitance signal for $\varepsilon_a / \varepsilon_w = 0.05$ in concentric annular flow

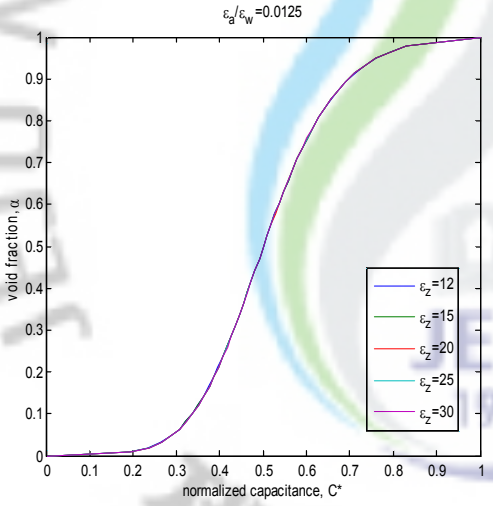

Void fraction, α	$\left\|\frac{C^*_{\varepsilon_z=12} - C^*_{\varepsilon_z=30}}{C^*_{\varepsilon_z=12}}\right\|$
0.1	0.0022
0.2	0.0018
0.3	0.0012
0.4	0.0015
0.5	0.0002
0.6	0.0006
0.7	0.0002
0.8	0.0006
0.9	0.0002

Figure 25: Effect of temperature-dependent insulator on capacitance signal for $\varepsilon_a / \varepsilon_w = 0.0125$ in stratified flow

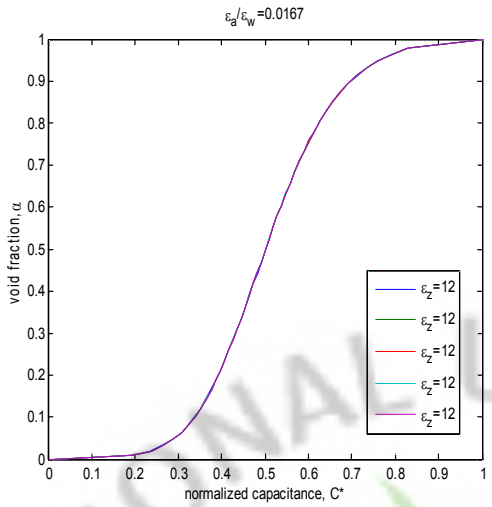

Void fraction, α	$\left\|\frac{C^*_{\varepsilon_z=12} - C^*_{\varepsilon_z=30}}{C^*_{\varepsilon_z=12}}\right\|$
0.1	0.0049
0.2	0.0013
0.3	0.0016
0.4	0.0004
0.5	0.0007
0.6	0.0010
0.7	0.0007
0.8	0.0004
0.9	0.0014

Figure 26: Effect of temperature-dependent insulator on capacitance signal for $\varepsilon_a / \varepsilon_w = 0.0167$ in stratified flow

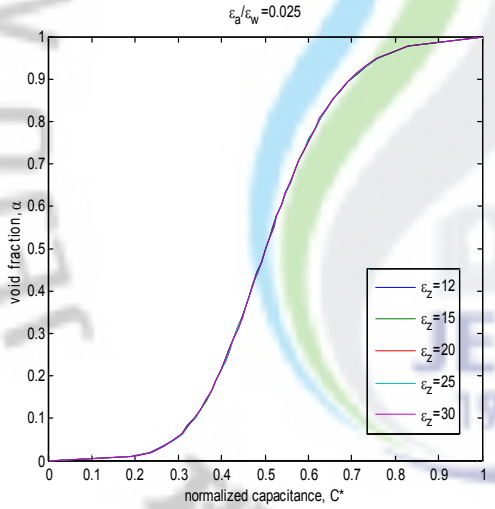

Void fraction, α	$\left\|\frac{C^*_{\varepsilon_z=12} - C^*_{\varepsilon_z=30}}{C^*_{\varepsilon_z=12}}\right\|$
0.1	0.0025
0.2	0.0002
0.3	0.0034
0.4	0.0003
0.5	0.0008
0.6	0.0005
0.7	0.0018
0.8	0.0012
0.9	0.0007

Figure 27: Effect of temperature-dependent insulator on capacitance signal for $\varepsilon_a / \varepsilon_w = 0.025$ in stratified flow

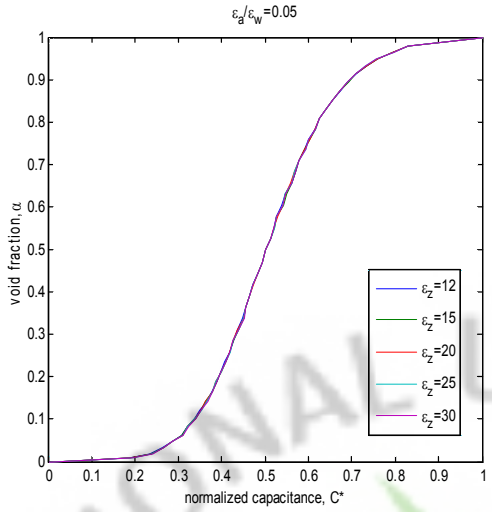

Void fraction, α	$\left\|\frac{C^*_{\varepsilon_z=12} - C^*_{\varepsilon_z=30}}{C^*_{\varepsilon_z=12}}\right\|$
0.1	0.0035
0.2	0.0019
0.3	0.0039
0.4	0.0006
0.5	0.0002
0.6	0.0018
0.7	0.0008
0.8	0.0013
0.9	0.0018

Figure 28: Effect of temperature-dependent insulator on capacitance signal for $\varepsilon_a / \varepsilon_w = 0.05$ in stratified flow

According to simulation results, the temperature-dependent behavior of the insulator does not significantly affect the normalized capacitance for given void fraction even though this work uses a simple assumption. For all cases maximum deviation between the normalized capacitance for $\varepsilon_z = 12$ and $\varepsilon_z = 30$ is less than 0.1%. This implies that impedance method is feasible even if the system is under severe conditions of high temperature and pressure which leads to change in permittivity of the insulator.

(3) Effect of the temperature-dependent behavior of water on capacitance signal

In the previous section the assessment of the effect of temperature-dependent insulator on capacitance signal was handled. This section, similarly, deals with the effect of temperature-dependent characteristic of the water on capacitance responses for given relative permittivity of the insulator, that is, $\varepsilon_z = 12,\ 15,\ 20,\ 25$, and 30.

Figures 29~38 show the deviation between the normalized capacitance for $\lambda = 0.0125$ which is conventional value at standard temperature and pressure and for $\lambda = 0.05$ at 550k and 10MPa with respect to given permittivity values of the insulator.

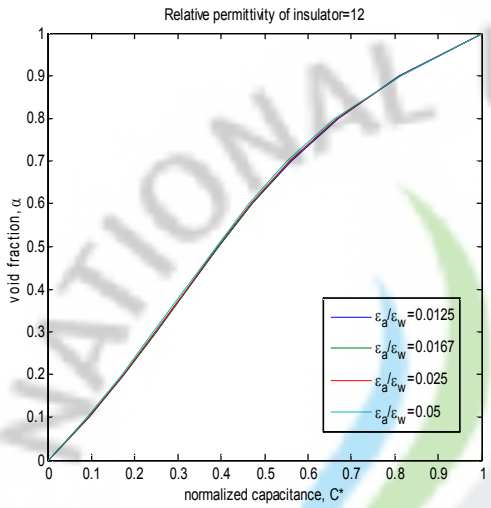

Void fraction, α	$\left\lvert \frac{C^*_{\lambda_c=0.0125} - C^*_{\lambda_c=0.05}}{C^*_{\lambda_c=0.0125}} \right\rvert$
0.1	0.0394
0.2	0.0324
0.3	0.0256
0.4	0.0225
0.5	0.0156
0.6	0.0169
0.7	0.0151
0.8	0.0116
0.9	0.0050

Figure 29: Effect of temperature-dependent permittivity of water on capacitance signal for $\varepsilon_z = 12$ in concentric annular flow

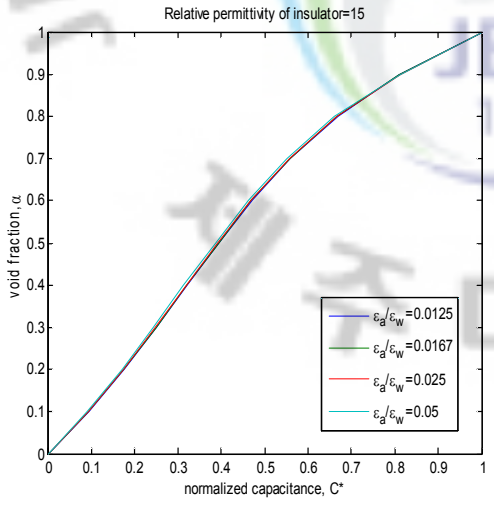

Void fraction, α	$\left\lvert \frac{C^*_{\lambda_c=0.0125} - C^*_{\lambda_c=0.05}}{C^*_{\lambda_c=0.0125}} \right\rvert$
0.1	0.0314
0.2	0.0302
0.3	0.0280
0.4	0.0254
0.5	0.0220
0.6	0.0191
0.7	0.0150
0.8	0.0126
0.9	0.0025

Figure 30: Effect of temperature-dependent permittivity of water on capacitance signal for $\varepsilon_z = 15$ in concentric annular flow

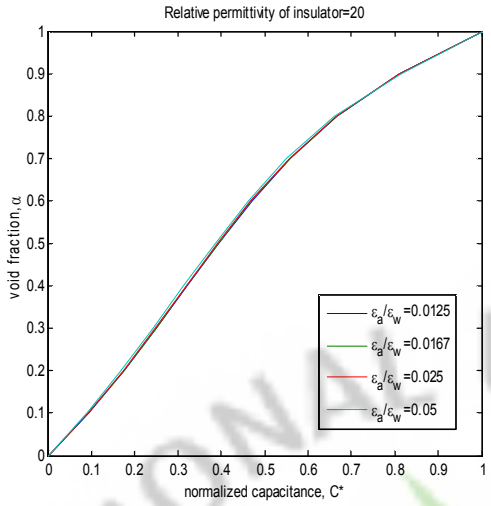

Void fraction, α	$\left\lvert \frac{C^*_{\lambda_c=0.0125} - C^*_{\lambda_c=0.05}}{C^*_{\lambda_c=0.0125}} \right\rvert$
0.1	0.0430
0.2	0.0349
0.3	0.0266
0.4	0.0253
0.5	0.0220
0.6	0.0192
0.7	0.0173
0.8	0.0104
0.9	0.0058

Figure 31: Effect of temperature-dependent permittivity of water on capacitance signal for $\varepsilon_z = 20$ in concentric annular flow

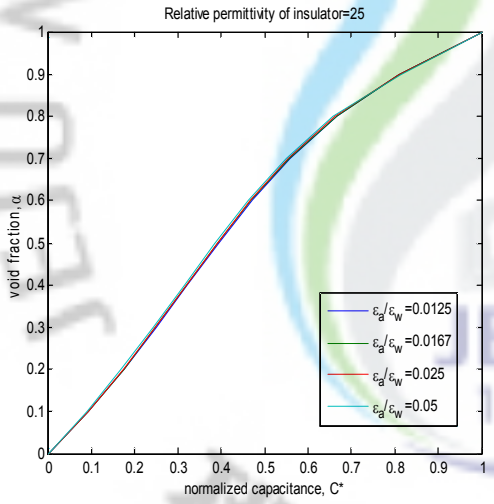

Void fraction, α	$\left\lvert \frac{C^*_{\lambda_c=0.0125} - C^*_{\lambda_c=0.05}}{C^*_{\lambda_c=0.0125}} \right\rvert$
0.1	0.0389
0.2	0.0331
0.3	0.0278
0.4	0.0208
0.5	0.0216
0.6	0.0170
0.7	0.0178
0.8	0.0128
0.9	0.0041

Figure 32: Effect of temperature-dependent permittivity of water on capacitance signal for $\varepsilon_z = 25$ in concentric annular flow

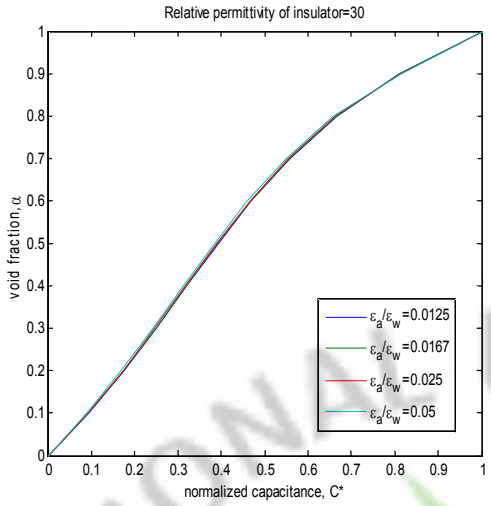

Void fraction, α	$\left\lvert \frac{C^*_{\lambda_c=0.0125} - C^*_{\lambda_c=0.05}}{C^*_{\lambda_c=0.0125}} \right\rvert$
0.1	0.0494
0.2	0.0371
0.3	0.0283
0.4	0.0259
0.5	0.0226
0.6	0.0204
0.7	0.0168
0.8	0.0146
0.9	0.0056

Figure 33: Effect of temperature-dependent permittivity of water on capacitance signal for $\varepsilon_z = 30$ in concentric annular flow

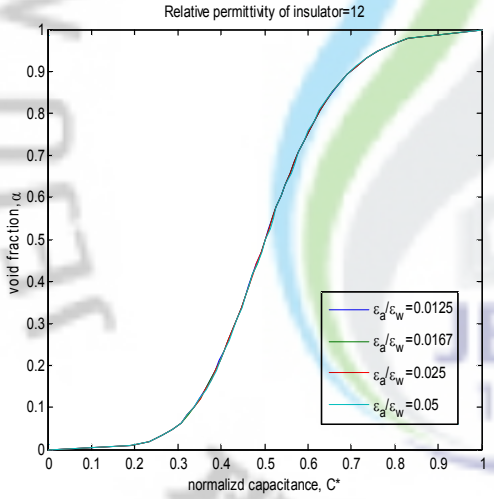

Void fraction, α	$\left\lvert \frac{C^*_{\lambda_c=0.0125} - C^*_{\lambda_c=0.05}}{C^*_{\lambda_c=0.0125}} \right\rvert$
0.1	0.00001
0.2	0.00244
0.3	0.00159
0.4	0.00402
0.5	0.00015
0.6	0.00389
0.7	0.00102
0.8	0.00136
0.9	0.00140

Figure 34: Effect of temperature-dependent permittivity of water on capacitance signal for $\varepsilon_z = 12$ in stratified flow

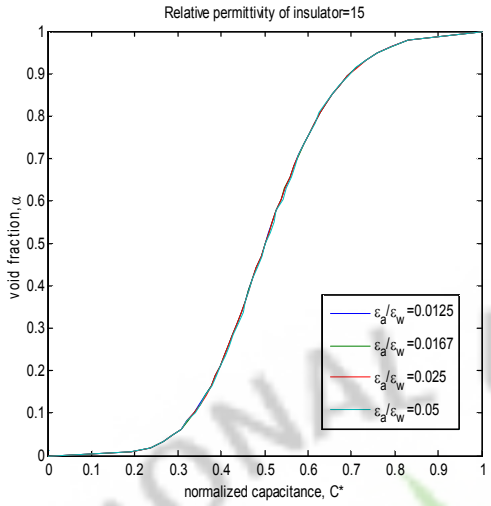

Void fraction, α	$\left\lvert \frac{C^*_{\lambda_c=0.0125} - C^*_{\lambda_c=0.05}}{C^*_{\lambda_c=0.0125}} \right\rvert$
0.1	0.0071
0.2	0.0045
0.3	0.0047
0.4	0.0030
0.5	0.0005
0.6	0.0080
0.7	0.0019
0.8	0.0027
0.9	0.0011

Figure 35: Effect of temperature-dependent permittivity of water on capacitance signal for $\varepsilon_z = 15$ in stratified flow

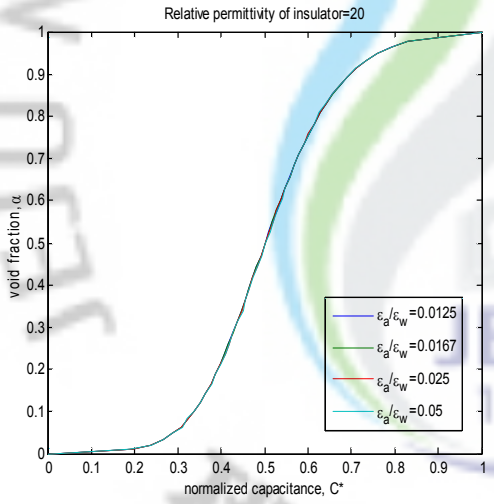

Void fraction, α	$\left\lvert \frac{C^*_{\lambda_c=0.0125} - C^*_{\lambda_c=0.05}}{C^*_{\lambda_c=0.0125}} \right\rvert$
0.1	0.0018
0.2	0.0060
0.3	0.0033
0.4	0.0043
0.5	0.0008
0.6	0.0039
0.7	0.0010
0.8	0.0009
0.9	0.0015

Figure 36: Effect of temperature-dependent permittivity of water on capacitance signal for $\varepsilon_z = 20$ in stratified flow

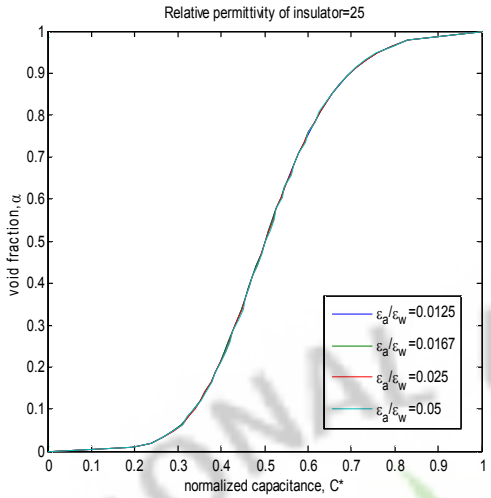

Void fraction, α	$\left\|\frac{C^*_{\lambda_c=0.0125}-C^*_{\lambda_c=0.05}}{C^*_{\lambda_c=0.0125}}\right\|$
0.1	0.0006
0.2	0.0050
0.3	0.0044
0.4	0.0032
0.5	0.0001
0.6	0.0052
0.7	0.0019
0.8	0.0019
0.9	0.0009

Figure 37: Effect of temperature-dependent permittivity of water on capacitance signal for $\varepsilon_z = 25$ in stratified flow

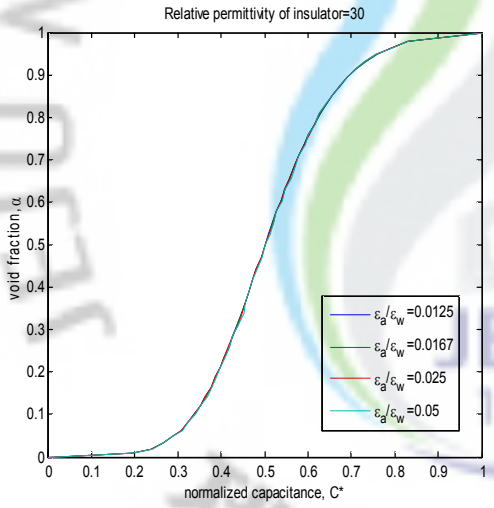

Void fraction, α	$\left\|\frac{C^*_{\lambda_c=0.0125}-C^*_{\lambda_c=0.05}}{C^*_{\lambda_c=0.0125}}\right\|$
0.1	0.0013
0.2	0.0025
0.3	0.0042
0.4	0.0031
0.5	0.0003
0.6	0.0051
0.7	0.0015
0.8	0.0019
0.9	0.0029

Figure 38: Effect of temperature-dependent permittivity of water on capacitance signal for $\varepsilon_z = 30$ in stratified flow

In these simulations maximum deviation between capacitance for $\lambda = 0.0125$ and $\lambda = 0.05$ is approximately 5% in case of concentric annular flow, on the other hand, that of stratified flow is less than 0.1%. In case of stratified flow the geometric effect appears to be more dominant than the change in relative permittivity of water. This is because the sensors are

completely surrounded by water which goes through severe variation of permittivity in concentric annular flow, while in stratified flow the sensors are partially submerged in water.

From the previous section and the foregoing discussion it is confirmed that the temperature-dependent behavior of the insulator and water does not have any significant effects on the normalized capacitance-void fraction relationship. However, it should be noted that calculated capacitance ratio which is defined as Eq. (12) is quite different. This ratio is a very important parameter offering the information for the experimental calibration. Table 7 shows calculated capacitance ratio for various permittivity values of the insulator and water which are used in simulations.

Table 7: Capacitance Ratio (C_a / C_w) for given permittivity values of the insulator and water

Permittivity Ratio, λ	Capacitance Ratio (C_a / C_w) for given permittivity values of insulator				
	12	15	20	25	30
0.0125	0.265	0.309	0.372	0.424	0.468
0.0167	0.325	0.374	0.442	0.496	0.541
0.025	0.421	0.475	0.544	0.598	0.640
0.05	0.598	0.649	0.710	0.752	0.784

Considering the air-water or steam-water two phase flow, the permittivity ratio $\lambda = 0.05$ at 550k and 10MPa, and the relative permittivity value of the insulator may increase up to 20 or so on. For these cases the impedance method may require more sophisticated measurements which can detect the void fraction existing in small deviation between capacitance value for $\alpha = 1$ and $\alpha = 0$, which corresponds to large C_a / C_w.

VII. Conclusions

For the application of the impedance method to void fraction measurements theoretical relationship between the normalized capacitance or resistance and void fraction for concentric annular flow and stratified flow is proposed. In this relationship the sensor size is one of most significant parameters along with the electrical properties of the domain. Various simulations are performed to determine the optimal sensor size changing the angle between sensors. As the sensor size increases the sensitivity of the sensor for void fraction measurement based on the normalized capacitance or resistance tends to be higher, on the other hand, the relationship between the normalized capacitance or resistance and void fraction becomes linear with decrease in the sensor size. This theoretical relationship is compared with static experiments. On the whole, experimental results match the predicted signal, however, some errors occur in low void fraction regions for both cases, the concentric annular and stratified flow. These errors are thought to be caused by the contact impedance which is not considered in the theoretical relationship. In this work, main considerations for accurate assessment of the void fraction based on real geometry of the sensor which are designed by KAERI are also handled. These considerations are classified in three parts: (1) effect of the insulator, (2) effect of the temperature-dependent insulator, (3) effect of the temperature-dependent permittivity of the water on capacitance signal.

Simulation results show that the effect of the insulator is slightly large, roughly 5% for both the concentric annular flow and stratified flow, but that of temperature-dependent behavior of the insulator and water is negligible if sophisticated measurements are devised.

This works use many assumptions as follows:

(1) Theoretical relationship is derived for ideal concentric annular flow and stratified flow without any fluctuations of the interface between the water and air region.

(2) No contact impedance is considered for both concentric annular and stratified flow.

(3) Temperature-dependent behavior of the insulator and water is assumed to be constant.

For the development of the sensor for monitoring the void fraction further study may deal with the following tasks:

(1) Verification of feasibility of impedance method for real situations:

- Eccentric annular flow
- Distorted bubble
- Bubbly flow
- Slug type flow
- Wavy flow

(2) Development of the model considering the effect of the contact impedance and temperature-dependent behavior of components and fluid in the sensor module.

References

Chakraborty S, Keller E, Talley J, Srivastav A, Ray A and Kim S (2009), Void fraction measurement in two-phase flow processes via symbolic dynamic filtering of ultrasonic signals, Meas. Sci. Technol. 20 023001.

Devia F and Fossa M (2003), Design and optimization of impedance probes for void fraction measurements, Flow Meas. Instrum. 9 103-9.

Elkow K J and Rezkallah K S (1996) Void fraction measurements in gas-liquid flows using capacitance sensors, Meas. Sci. Technol. 7 1153-63.

Kendoush A A (1992) A comparative study of the various nuclear radiations used for void fraction measurements, Nucl. Eng. Des. 137 249-57.

Kim J, Ahn Y-C and Kim M H (2009) Measurement of void fraction and bubble speed of slug flow with three-ring conductance probes, Flow Meas. Instrum. 20 103-9.

Shu M T, Weinberger C B and Lee Y H (1982) A simple capacitance sensor for void fraction measurement in two-phase flow, Ind. Eng. Chem. Fundam. 21 181-2.

Ursenbacher T, Wojtan L and Thome J R (2004) Interfacial measurements in stratified types of flow: Part I. New optical measurement technique and dry angle measurements, Int. J. Multiph. Flow. 30 107-24.

Wojtan L, Uresenbacher T and Thome J R (2004), Interfacial measurements in stratified types of flow: Part Ⅱ. Measuremets for R-22 and R-410 A, Int. J. Multiph. Flow. 30 107-24.

Sin Kim, Jeong Seong Lee, Kyung Youn Kim, Kyung Ho Kang and Byung Jo Yun(2009) An approximate formula for the capacitance-void fraction relationship for annular flows, Meas. Sci.

Technol. 20 125404.

Chul Hwa Song, Moon Ki Chung and Hee Cheon No (1998) Measurement of void fraction by an improved multi-channel conductance void meter, Nucl. Eng. Des. 184 269-285.

H.V. Kok, W.C. Heerens, T.H.J.J. van der Hagen and H. van Dam (1995) A new principle for designing optimal capacitive void fraction sensors applied to a rod-bundle geometry, Meas. 15 119-131.

Gui-Bo Zheng, Ning-De Jin, Xiao-Hui Jia, Peng-Ju Lv and Xing-Bin Liu (2008) Gas-liquid two phase flow measurement method based on combination instrument of turbine flowmeter and conductance sensor, Int. J. Multiph. Flow. 34 1031-1047.

Wael H. Ahmed (2006) Capacitance Sensor for Void-Fraction Measurements and Flow-Pattern Identification in Air-Oil Two-Phase Flow, IEEE SENSORS JOURNAL, VOL. 6, NO. 5.

A. Jaworek, A. Krupa and M. Trela (2004) Capacitance sensor for void fraction measurement in water/steam flows, Flow Meas. Instrum. 15 317-324.

H.C. Yang, D.K. Kim and M.H. Kim (2003) Void fraction measurement using impedance method, Flow Meas. Instrum. 14 151-160.

Baek et al. (2009) Thermal Hydraulic Integral Effect Tests for APR1400/OPR1000 Accidents, KAERI/RR-3103/2009, Korea Atomic Energy Research Institute.

감사의 글

감사의 글을 쓰려고 하니 2년 동안 경험했던 몇 번(?)의 고비와 환희가 머릿속을 스쳐 갑니다. 지금까지 논문을 쓰면서 많은 분들의 도움이 있었습니다. 이제 논문을 정리하면서 그 동안 격려해주시고 도움을 베풀어 주신 분들께 감사의 인사를 드리고자 합니다.

먼저, 연구실 생활 해본 적 없는 저에게 늘 용기와 격려를 아끼지 않으셨던 김신 교수님께 머리 숙여 깊이 감사드립니다. 또한 연구실 회의 시간에 항상 좋은 말씀해주신 김경연 교수님께도 깊이 감사드립니다. 원자력에 대한 시야를 넓혀 주신 정범진 교수님께도 깊이 감사드립니다. 그리고 원자력연구원의 송철화 박사님, 윤병조 박사님, 강경호 박사님께도 진심으로 감사드립니다.

2년 동안 연구실에서 동거동락 했던 이보안 선배, 이정성 선배, 성용, 윤정, 아름, 송혜령 선생님, 롱리, 무르투자, 노만, 그리고 에너지 공학과 대학원 선후배 준호형, 지훈이형, 상범이형, 봉진이형, 승진이형, 성식, 향민, 영민, 원종, 경욱, 정환, 재경, 세민, 태영, 그리고 동기 민우, 민국에게도 진심으로 감사드립니다. 또한 연구실 회의 때 아낌없는 조언과 관심 가져주신 김봉석 선배, 애마르, 아닐, 유동에게도 감사드립니다.

끝으로 느지막이 공부 시작한다고 걱정 많이 하셨지만 묵묵히 믿고 응원해주신 아버지, 어머니, 형들, 누나들, 매형들에게 이루 말할 수 없는 감사의 마음을 전합니다. 그리고 석사 공부 즐겁게 할 수 있게 항상 밝은 웃음 보여준 MS에게 감사와 사랑의 마음을 전합니다. 앞으로 더 열심히 살겠습니다.